Journal of Applied Physics

Absolute Seebeck coefficient of thin platinum films

Cite as: J. Appl. Phys. **126**, 105106 (2019); https://doi.org/10.1063/1.5101028
Submitted: 26 April 2019 . Accepted: 20 August 2019 . Published Online: 09 September 2019

M. Kockert, R. Mitdank, A. Zykov, S. Kowarik, and S. F. Fischer

Journal of Applied Physics ARTICLE scitation.org/journal/jap

Absolute Seebeck coefficient of thin platinum films

Cite as: J. Appl. Phys. **126**, 105106 (2019); doi: 10.1063/1.5101028
Submitted: 26 April 2019 · Accepted: 20 August 2019 ·
Published Online: 9 September 2019

M. Kockert,[1,a)] R. Mitdank,[1] A. Zykov,[2] S. Kowarik,[2,3] and S. F. Fischer[1,b)]

AFFILIATIONS

[1]Novel Materials Group, Humboldt-Universität zu Berlin, Berlin 10099, Germany
[2]Nanoscale Processes and Growth, Humboldt-Universität zu Berlin, Berlin 10099, Germany
[3]Bundesamt für Materialforschung und -prüfung (BAM), Berlin 12203, Germany

[a)]**Electronic mail:** kockert@physik.hu-berlin.de
[b)]**Electronic mail:** saskia.fischer@physik.hu-berlin.de

ABSTRACT

The influence of size effects on the thermoelectric properties of thin platinum films is investigated and compared to the bulk. Structural properties, like the film thickness and the grain size, are varied. We correlate the electron mean free path with the temperature dependence of the electrical conductivity and the absolute Seebeck coefficient S_{Pt} of platinum. A measurement platform was developed as a standardized method to determine S_{Pt} and show that $S_{Pt,film}$ is reduced compared to $S_{Pt,bulk}$. Boundary and surface scattering reduce the thermodiffusion and the phonon drag contribution to $S_{Pt,film}$ by nearly the same factor. We discuss in detail on behalf of a model, which describes the temperature dependence of the absolute Seebeck coefficient, the influence of size effects of electron-phonon and phonon-phonon interaction on S_{Pt}.

I. INTRODUCTION

Platinum is the most commonly used thermoelectric reference material and is used with other materials, e.g., as commercially available bulk thermocouples.[1] However, in recent years, micro- and nanopatterning have become more interesting.[2,3] Popular examples are thin films[4,5] and nanowires.[6,7] New challenges for metrology and its interpretation are coming with this trend.

In order to determine the thermoelectric transport properties of nanowires, measurements are usually performed relative to thin films.[6–9] For this purpose, microelectromechanical systems (MEMS) with thin platinum conduction lines of a few hundred nanometer thickness have been developed as measurement platforms.[10–12] However, thin metal films have a reduced absolute Seebeck coefficient S_{film} compared to the bulk S_{bulk}.[13–18] Specifically for metal-metal junctions, it is important to know the absolute Seebeck coefficient of the reference material. Deviations in the single-digit microvolt per Kelvin range can easily lead to misinterpretations of the measurement results.

For this reason, we present a measurement platform to investigate the temperature-dependent thermoelectric transport properties of thin metal films and demonstrate its usability by investigating platinum films with a thickness of 134 nm and 197 nm. To understand the influence of the microstructure on the absolute Seebeck coefficient S, we adapted and improved a model[19,20] that allows the decomposition of S into a thermodiffusion and a phonon drag contribution. The influence of the electron-phonon interaction compared to the phonon-phonon interaction on the phonon drag part of $S_{Pt,film}$ and $S_{Pt,bulk}$ is discussed. This work shows that thin platinum films differ significantly from the bulk in terms of S by nearly 400% at $T = 290$ K.

II. EXPERIMENTAL DETAILS

A thermoelectric micro lab (TML) was designed with microlithography on a $5 \times 9\,\mathrm{mm}^2$ glass substrate and it is shown in Fig. 1(a). The TML involves a thermocouple, which consists of a thin sputtered platinum film (sputter target: 99.99% platinum) and an attached bulk gold wire (diameter: 25 μm, purity: 99.99%). This bulk gold wire creates a thermoelectric connection between the upper and lower part of the platinum film. A platinum line heater is used to generate a temperature difference δT between the hot

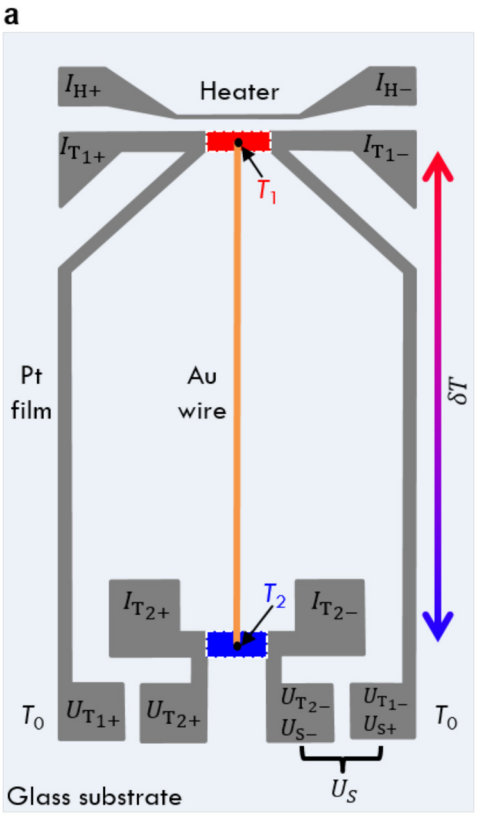

FIG. 1. Sketches of the measurement setup. (a) Sketch of the thermoelectric microlab. Platinum (Pt) was sputtered on a $(5 \times 9)\,\mathrm{mm}^2$ glass substrate. A line heater creates a temperature difference $\delta T = T_1 - T_2$ between the hot (temperature T_1, red) and cold (temperature T_2, blue) contacts by applying a current at the contacts I_{H+} and I_{H-}. A bulk gold (Au) wire (diameter $d = 25\,\mu\mathrm{m}$) was bonded at the hot and cold four-terminal resistance thermometers indicated by the corresponding current contacts (I_{T_1}, I_{T_2}) and voltage contacts (U_{T_1}, U_{T_2}). The thermovoltage U_S was measured at the Pt pads with respect to the cold side of the sample. The Pt pads were kept at the same temperature T_0 in order to minimize parasitic thermovoltages. (b) Sketch of the measurement setup as a thermocouple consisting of bulk gold (Au) and platinum (Pt). A temperature difference along both materials resulting from different junction temperatures ($T_1 > T_2$) between Au and Pt produces a thermovoltage U_S.

(temperature T_1, red) and cold (temperature T_2, blue) contacts. The temperatures at the hot contact and the cold contact are determined by four-terminal resistance thermometers. The resulting temperature difference along both materials due to the different junction temperatures ($T_1 > T_2$) produces a thermovoltage U_S. The relative Seebeck coefficient between the bulk gold wire and the thin platinum film with respect to the cold side is given by

$$S_{\mathrm{Au,Pt}} = -\frac{\mathrm{d}U_{S_{\mathrm{Au,Pt}}}}{\mathrm{d}\delta T}. \tag{1}$$

Here, we prepared and investigated platinum films with a thickness of 134 nm and 197 nm. After the thermoelectric characterization of the samples in a flow cryostat in helium atmosphere at ambient pressure, a heat treatment was performed on the same samples. The heat treatment was carried out in a rapid thermal annealer in vacuum. The temperature of the annealer was gradually increased from 115 °C to 250 °C and finally to a maximum of 400 °C. The temperature plateaus were held for two minutes each. A thermoelectric characterization of the same samples was performed after the heat treatment. For the X-ray investigations, $10 \times 10\,\mathrm{mm}^2$ large samples were prepared according to the same procedure with a thickness of 139 nm and 203 nm. X-ray experiments have been conducted with a lab-based diffractometer, with a Cu-K_α rotating anode source with a wavelength of $\lambda = 0.154\,\mathrm{nm}$. The thickness of all samples was determined by atomic force microscopy.

III. RESULTS

A. X-ray

X-ray measurements of polycrystalline platinum films with thicknesses of 139 nm and 203 nm exhibit four Bragg peaks corresponding to the platinum (111), (200), (220), and (311) reflections. The most intense Bragg peak of the 203 nm thin film is the (111) reflection [see Fig. 2(a)], indicating a preferential orientation of the crystallites with a surface parallel (111) plane. Additional heat treatment and increased temperature of the heat treatment lead to an increase in the peak intensity and a shift of the peak position to larger detector angles. The position of the Bragg reflection at (111) of the annealed platinum films is in agreement with the literature.[21] The average crystallographic grain size D_S of the crystallites with a (111) orientation was estimated by the Scherrer equation[22,23]

$$D_S \geq \frac{K\lambda}{\Delta(2\theta)\cos(\theta)}. \tag{2}$$

Here, K is a dimensionless shape factor with a value of 0.9, $\lambda = 0.154\,\mathrm{nm}$ is the X-ray wavelength. The broadening $\Delta(2\theta)$ is given by the full-width at half-maximum FWHM of the X-ray diffraction peak shown in Fig. 2(a) and θ is the Bragg angle. D_S of 139 nm and 203 nm from as sputtered thin platinum films are $D_{S,139\,\mathrm{nm}} \geq (33 \pm 2)\,\mathrm{nm}$ and $D_{S,203\,\mathrm{nm}} \geq (35 \pm 2)\,\mathrm{nm}$, respectively. This size increases with heat treatment at 400 °C to $D_{S,139\,\mathrm{nm,400C}} \geq (41 \pm 1)\,\mathrm{nm}$ and $D_{S,203\,\mathrm{nm,400C}} \geq (41 \pm 1)\,\mathrm{nm}$, respectively.

Furthermore, the mosaicity Γ, which is a measure of the spread of crystal plane orientations, was determined for the (111) Bragg reflection. Figure 2(b) shows a rocking scan where the

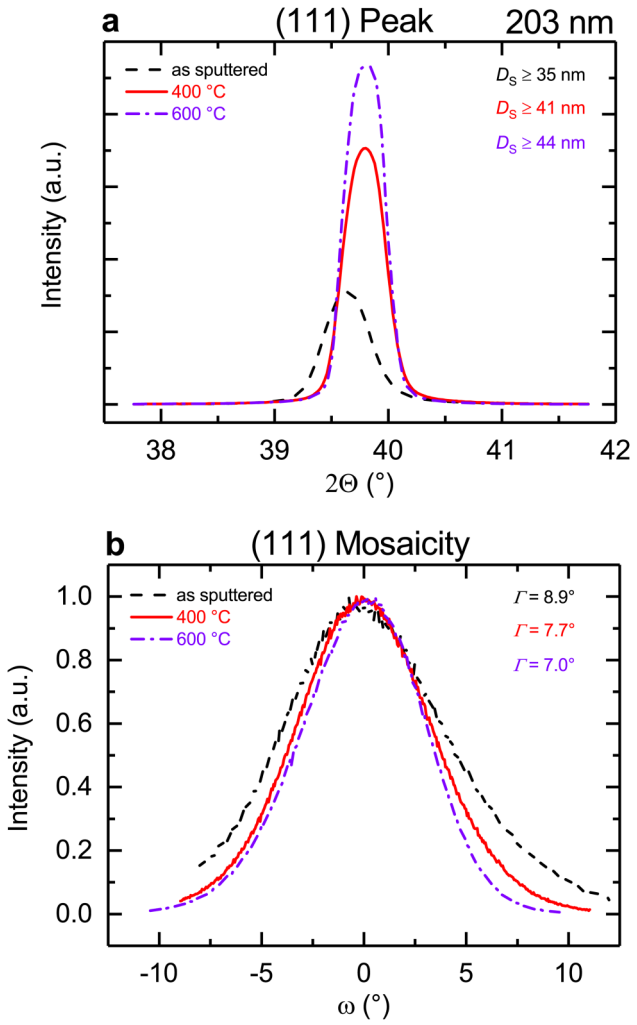

FIG. 2. X-ray diffractometry of a thin platinum film with a thickness of 203 nm as sputtered and with additional heat treatment. (a) Intensity of the (111) Bragg reflection as a function of detector angle 2Θ as sputtered, with heat treatment at a maximum temperature of 400 °C and 600 °C. The average crystallographic grain size D_S was determined by the Scherrer equation. (b) Intensity of the (111) Bragg peak as a function of the rocking angle variation ω as sputtered, with heat treatment at a maximum temperature of 400 °C and 600 °C. The mosaicity Γ of the platinum crystallites with a (111) texture is given by the full width at half-maximum of the peak.

sample angle ω is varied for a fixed detector angle 2θ. As the (111) lattice planes are not all perfectly parallel to the substrate surface, the intensity is found within an angular distribution of FWHM Γ. Γ of 139 nm and 203 nm as-sputtered thin platinum films are $\Gamma_{139\,nm} = (11.0 \pm 0.4)^\circ$ and $\Gamma_{203\,nm} = (8.9 \pm 0.2)^\circ$, respectively. Thicker platinum films, therefore, have a more perfect texture corresponding to a narrower distribution of crystallite tilt angles. The tilt decreases and so the crystal quality increases with heat treatment at 400 °C to $\Gamma_{139\,nm,400\,°C} = (9.5 \pm 0.2)^\circ$ and $\Gamma_{203\,nm,400\,°C} = (7.7 \pm 0.2)^\circ$, respectively.

B. Electrical measurements

The Bloch-Grüneisen equation was used to fit the temperature-dependent resistance of the platinum films, which show the expected metallic behavior given in Fig. 3(a), in order to determine the Debye temperature Θ_D of the material. All platinum films with heat treatment and the bulk material (wire diameter $d = 25\,\mu m$) agree with the literature value of $\Theta_D = 240$ K.[24] Pt 3 (197 nm, without heat treatment) has a reduced Debye temperature $\Theta_{D,Pt\,3} = 191$ K compared to the literature. This can be attributed to the microstructure.

Furthermore, the residual resistance ratio *RRR* was determined as the ratio of the resistance at 290 K divided by the resistance of 20 K in order to compare the quality of the sputtered platinum films and the influence of the heat treatment. Bulk platinum has the highest residual resistance ratio $RRR_{bulk} = 50.3 \pm 0.1$. Thin films have a reduced residual resistance ratio compared to the bulk given in Table I.

Figure 3(b) shows the temperature coefficient α of the resistance of platinum. The temperature coefficient of resistance is given by the derivative of the resistivity of platinum to the temperature,[25–27]

$$\alpha = \frac{1}{\rho}\frac{d\rho}{dT}. \tag{3}$$

For thin films, α depends on the thickness of the platinum films. Larger film thickness and additional heat treatment lead to an increase of the temperature coefficient. The four-terminal resistance of the cold thermometer was used to determine the electrical conductivity σ of the thin platinum films shown in Fig. 3(c). The electrical conductivity of the platinum bulk wire σ_{bulk} is larger than σ_{film}. σ_{film} depends on the film thickness, which can be increased by heat treatment and reaches a maximum at low bath temperatures.

Figure 3(d) features the electron mean free path Λ_{el} of the thin films and of the bulk. The electron mean free path of the thin films is reduced compared to the bulk and increases with increasing film thickness and can be further increased by heat treatment. At low bath temperatures, the mean free path reaches a maximum limited by the film thickness and the structural properties.

C. Seebeck measurements

In addition to the electrical characterization, the temperature-dependent Seebeck coefficient of thin platinum films and bulk platinum relative to a bulk gold wire (wire diameter $d = 25\,\mu m$) was determined by measuring the thermovoltage U_S as a function of the heater current of the line heater. Figure 4 shows the parabolic behavior of the thermovoltage indicating the thermoelectric effect. The temperature difference δT was determined by four-terminal resistance measurements of the thermometers at the hot and cold sides of the measurement platform. The slope of the function $U_S(\delta T)$ gives the relative Seebeck coefficient,

$$S_{Au,Pt} = S_{Au} - S_{Pt} = -\frac{dU_{S_{Au,Pt}}}{d\delta T}. \tag{4}$$

The relative Seebeck coefficient of the thin films and the bulk material decreases with decreasing bath temperature as depicted in

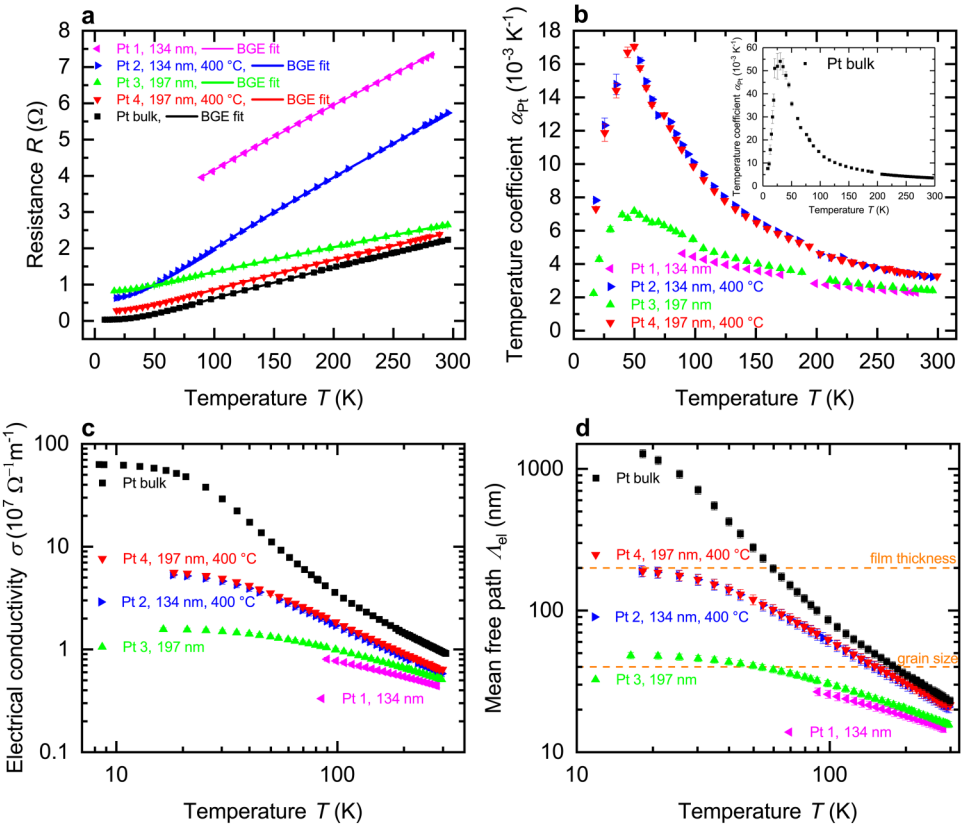

FIG. 3. Electrical measurements of thin platinum films as-sputtered and with heat treatment and of the bulk. (a) Four-terminal resistance R as a function of the bath temperature T. The Bloch-Grüneisen equation (BGE) was fitted to the data in order to determine the temperature dependence of the resistance and to calculate the Debye temperature. (b) Temperature coefficient α_{Pt} of the resistance as a function of the bath temperature T. The inset shows the temperature coefficient of the bulk material. (c) Electrical conductivity σ as a function of the bath temperature T. (d) Mean free path of the electrons Λ_{el} as a function of the bath temperature T. The mean free path of as-sputtered thin platinum films is mainly limited by grain boundaries at low temperatures. The mean free path of thin platinum films with heat treatment is mainly limited by the film thickness.

Fig. 5(a). In order to determine the absolute Seebeck coefficient of platinum S_{Pt}, the absolute Seebeck coefficient of bulk gold S_{Au} was taken from Ref. 28. S_{Pt} is given in Fig. 5(b).

IV. DISCUSSION

A. Structural and electrical characterization

X-ray diffraction analysis gives the average crystallographic grain size D_S, which was determined by the Scherrer equation[22,23] from the (111) Bragg reflections of Fig. 2(a). The determined values indicate only a lower limit for the crystallographic grain size. The actual grain size can be larger. Furthermore, the X-ray measurements only provide information about the grain size in the growth direction. The in-plane grain size can be significantly larger than the grain size in the growth direction. In addition to the average crystallographic grain size, the morphological grain size is discussed in the literature.[29–31] It was proposed that the morphological grains, which were determined by scanning tunneling microscopy, are agglomerates of crystallographic grains and that the morphological grain size is increasing with increasing film thickness much further than the crystallographic grain size.[29,30] Overall, X-ray diffraction analysis clearly exhibits that heat treatment increases the crystal quality of the thin platinum films. In addition to structural investigations, the residual resistance ratio *RRR* is an indicator of the crystal quality.[32–34] The *RRR* is increased after the heat treatment of thin platinum films confirming the improved crystal quality compared to thin films without heat treatment. Furthermore, the reduced electrical conductivity and the reduced temperature coefficient of the platinum thin films compared to the bulk are comparable with results reported in Refs. 25 and 35.

TABLE I. Thickness, heat treatment parameters, and residual resistance ratio. Overview of thickness t, maximum heat treatment temperature T_{max}, and residual resistance ratio *RRR* of four thin platinum films. The thickness was determined by atomic force microscopy. The residual resistance ratio *RRR* was determined as the ratio of the resistance at 290 K divided by the resistance of 20 K.

Sample	t (nm)	T_{max} (°C)	*RRR*
Pt 1	134 ± 5	…	…
Pt 2	134 ± 5	400	8.45 ± 0.01
Pt 3	197 ± 5	…	3.00 ± 0.01
Pt 4	197 ± 5	400	8.26 ± 0.01

The structural properties like film thickness and grain size are linked with the mean free path of the electrons in order to investigate the transport properties of the thin platinum films. The electron mean free path Λ_{el} was determined from the change of the electrical conductivity of the thin films under the assumption that scattering events reduce this length. This reduction of the

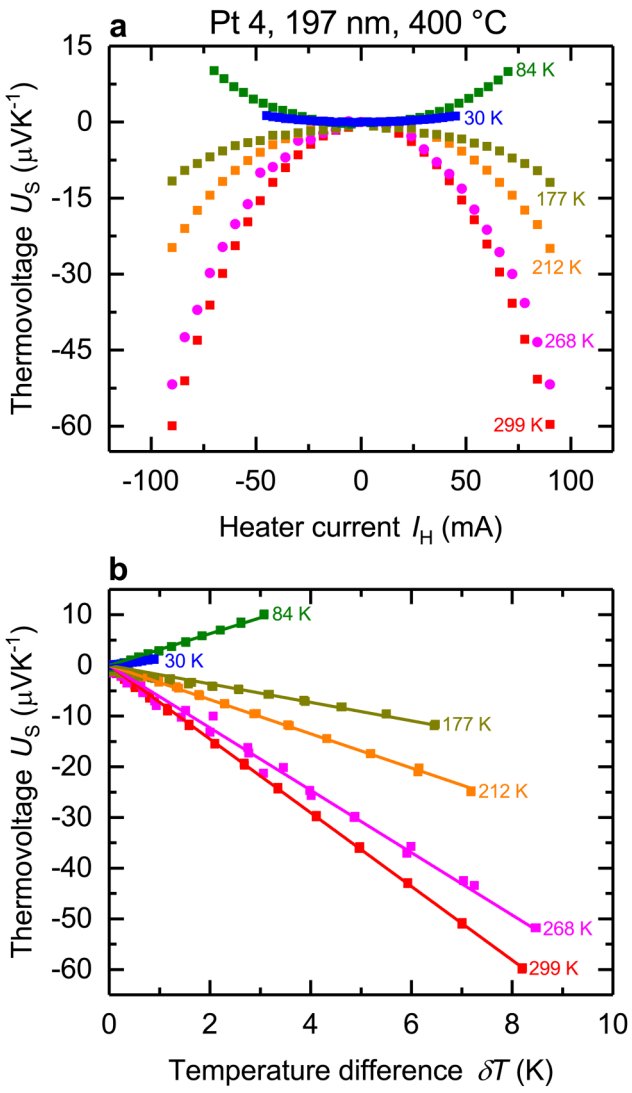

FIG. 4. Thermovoltage as a function of the heater current and temperature difference of Pt 4. (a) Thermovoltage U_S as a function of heater current I_H at different bath temperatures T. The sign of the thermovoltage changes below $T \approx 150$ K. (b) Thermovoltage U_S as a function of temperature difference δT at different bath temperatures T. The slope of the fitted solid lines gives the relative Seebeck coefficient between the thin platinum films and the bulk gold wire.

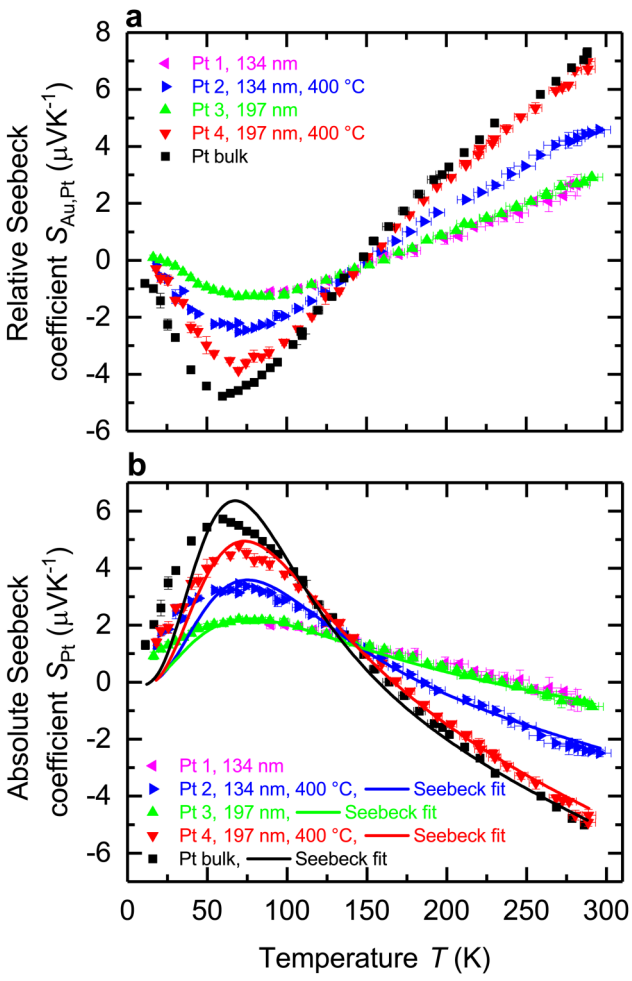

FIG. 5. Relative and absolute Seebeck coefficient of thin platinum films as sputtered and with heat treatment and bulk material. (a) Relative Seebeck coefficient $S_{Au,Pt}$ of platinum relative to a bulk gold wire with a diameter of 25 μm as a function of the bath temperature T. (b) Absolute Seebeck coefficient S_{Pt} of platinum as a function of the bath temperature T. The corresponding solid lines represent the Seebeck fit of the data. Absolute Seebeck coefficient of bulk gold S_{Au} was taken from Ref. 28.

electron mean free path can be described and related to the Matthiessen rule.[7]

$$\Lambda_{el,f}(T)^{-1} = \Lambda_{el,b}(T)^{-1} + \Lambda_{el,s,gb}^{-1} \tag{5}$$

is the inverse thin film electron mean free path, $\Lambda_{el,b}(T)^{-1}$ is the inverse mean free path of the bulk, and $\Lambda_{el,s,gb}^{-1}$ is the inverse temperature-independent scattering length of the electrons due to surface and grain boundary scattering.[7] The electrical conductivity is proportional to the mean free path and changes of the electrical conductivity affect the electron mean free path,

$$\sigma = en\mu = \frac{ne^2\tau}{m} = \frac{ne^2}{mv}\Lambda. \tag{6}$$

Here, e is the elementary charge, n is the charge carrier density, μ is the mobility, τ is the mean free time, m is the electron mass and v is the Fermi velocity.

$$\Lambda_{el,f}(T) = \frac{\sigma_f(T)}{\sigma_f(\mathrm{RT})}\Lambda_{el,f}(\mathrm{RT}) \tag{7}$$

TABLE II. Electron mean free path. Mean free path of the samples with thickness t and maximum heat treatment temperature T_{max}. $\Lambda_{el,f}(RT)$ is the electron mean free path of the thin films at room temperature and $\Lambda_{el,s,gb}$ is the temperature-independent mean free path of the electrons due to surface and grain boundary scattering. $\Lambda_{el,b}(RT) = 23$ nm of bulk is given in the literature at room temperature.[24]

Sample	t (nm)	T_{max} (°C)	$\Lambda_{el,f}(RT)$ (nm)	$\Lambda_{el,s,gb}$ (nm)
Pt 1	134	…	14 ± 1	36 ± 1
Pt 2	134	400	21 ± 2	212 ± 2
Pt 3	197	…	16 ± 1	48 ± 1
Pt 4	197	400	22 ± 2	219 ± 2

and

$$\Lambda_{el,b}(T) = \frac{\sigma_b(T)}{\sigma_b(RT)}\Lambda_{el,b}(RT) \tag{8}$$

are the electron mean free paths of the thin films and of the bulk material, respectively.[7] In order to determine $\Lambda_{el,f}(T)$, Eqs. (7) and (8) have to be combined with Eq. (5).[7] These relative changes of the electrical conductivities are fitted and yield the parameters $\Lambda_{el,f}(RT)$ and $\Lambda_{el,s,gb}$.[7] The electron mean free path of bulk platinum at room temperature $\Lambda_{el,b}(RT) = 23$ nm is given in Ref. 24 and has to be considered for the calculation.

Figure 3(d) shows the electron mean free path as a function of the bath temperature. Table II shows the electron mean free path at room temperature and the temperature-independent scattering length of the electrons. Pt 3 (197 nm, without heat treatment) has a mean free path, which saturates at low bath temperatures at $\Lambda_{el,s,gb} = (48 \pm 1)$ nm. Pt 2 (134 nm, with heat treatment) and Pt 4 (197 nm, with heat treatment) have nearly the same temperature dependence of the electron mean free path, which is in the order of magnitude of the film thickness. Heat treatment increases the mean free path. From the structural properties, we can conclude that the electron mean free path at low bath temperatures is mainly limited by grain boundaries for thin films without heat treatment. For thin films with heat treatment, the main limitation is set by the film thickness.

B. Seebeck coefficient

In general, the Seebeck coefficient is the sum of two parts: the thermodiffusion part and the phonon drag part,[14,19,20]

$$S = S_{diff} + S_{ph}. \tag{9}$$

Here, S_{diff} is the contribution due to the thermodiffusion of the charge carriers as described by Mott's formula,[14,20,36]

$$S_{diff} = \frac{\pi^2 k_B^2 T}{3e}\left(\frac{\partial \ln \sigma(\epsilon)}{\partial \epsilon}\right)\Big|_{\epsilon_F}, \tag{10}$$

where k_B is Boltzmann's constant, T is the bath temperature, e is the elementary charge, and $\frac{\partial \ln \sigma(\epsilon)}{\partial \epsilon}|_{\epsilon_F}$ is the derivative of the electrical conductivity according to the energy at the Fermi energy.

S_{ph} is the contribution due to the phonon drag effect. The phonon drag effect is based on the electron-phonon interaction. A momentum transfer from phonons to electrons leads to an increase of the Seebeck coefficient.[19] The phonon drag part of the Seebeck coefficient is connected with the specific heat of the phonons[19,20]

$$C_{ph(T)} = 9nk_B\left(\frac{T}{\Theta_D}\right)^3 \int_0^{\frac{\theta_D}{T}} \frac{x^4 \exp(x)}{(\exp(x)-1)^2}\,dx, \tag{11}$$

with the number of charge carriers per volume n and $x = \frac{\hbar\omega_D}{k_B T} = \frac{\Theta_D}{T}$ which is given by the reduced Planck's constant $\hbar$ and by the Debye frequency ω_D.

There are low and high temperature approaches to describe the phonon drag part of the Seebeck coefficient.[19] The low temperature approach can be described by $S_{ph} = \frac{C_{ph,low}}{3ne}$. According to the Debye model, the specific heat $C_{ph,low}$ goes with $T \to 0$ to $C_{ph,low} \propto T^3$ and for this reason $S_{ph,low} \propto T^3$.[19] The resulting Seebeck coefficient can be written as $S_{low} = S_{diff} + S_{ph,low} = aT + bT^3$. a and b are variables.

The high temperature approach has to be modified compared to the low temperature approach because the phonon-phonon scattering time τ_{pp} and the scattering time of the electron-phonon interaction τ_{ep} has to be taken into account.[19,20] The Debye model predicts a constant specific heat $\left(C_{ph,high} \approx 3nk_B\right)$ for temperatures above the Debye temperature Θ_D and due to phonon-phonon Umklapp scattering $S_{ph,high} \propto \frac{1}{T}$.[19] This results in $S_{high} = S_{diff} + S_{ph,high} = cT + d\frac{1}{T}$, where c and d are variables.

The combination of the low temperature approach, the high temperature approach, and additionally the characterization of the intermediate regime gives[19,20]

$$S_{ph} = \frac{C_{ph}(T)}{3ne}\gamma = \frac{C_{ph}(T)}{3ne}\frac{\tau_{pp}}{\tau_{pp}+\tau_{ep}}, \tag{12}$$

hence

$$S_{ph} = \frac{C_{ph}(T)}{3ne}\frac{1}{1+\frac{\tau_{ep}}{\tau_{pp}}} = \frac{C_{ph}(T)}{3ne}\frac{1}{1+F_\tau T\exp\left(-\frac{\Theta_D}{T}\right)}. \tag{13}$$

The relation $\frac{\tau_{ep}}{\tau_{pp}} = F_\tau T\exp\left(-\frac{\Theta_D}{T}\right)$ was suggested and adapted from Refs. 20 and 37. This equation assumes that the phonon-phonon interaction becomes dominant at high temperatures.[20,37] This results in the γ-factor,

$$\gamma = \frac{1}{1+\frac{\tau_{ep}}{\tau_{pp}}} = \frac{1}{1+F_\tau T\exp\left(-\frac{\Theta_D}{T}\right)}. \tag{14}$$

Finally, we combine the approach of the phonon drag part with the specific heat of the phonons and the thermodiffusion part $S_{diff} = F_{diff}\frac{T}{\Theta_D}$ to the formula, which describes the Seebeck coefficient over a wide temperature range,

$$S = F_{diff}\frac{T}{\Theta_D} + \frac{F_{ph}\left(\frac{T}{\Theta_D}\right)^3 \int_0^{\frac{\theta_D}{T}} \frac{x^4\exp(x)}{(\exp(x)-1)^2}\,dx}{1+F_\tau T\exp\left(-\frac{\Theta_D}{T}\right)}. \tag{15}$$

TABLE III. Seebeck fit parameters. Parameters of Seebeck fit for each sample with thickness t and maximum heat treatment temperature T_{max}. F_{ph} is the parameter that describes the intensity of the phonon drag part. F_τ gives the ratio of the scattering time of the electron-phonon interaction and of the phonon-phonon interaction. F_{diff} describes the intensity of the thermodiffusion part. $|F_{ph}/F_{diff}|$ gives the modulus ratio between the fit parameter of the thermodiffusion part and phonon drag part. S_{Pt} is the absolute Seebeck coefficient of platinum at 280 K. Due to the lack of low temperature data, the fit parameters of Pt 1 (197 nm, without heat treatment) are not given.

Sample	t (nm)	T_{max} (°C)	F_{ph} (μV K^{-1})	F_τ (K^{-1})	F_{diff} (μV K^{-1})	$\lvert F_{ph}/F_{diff}\rvert$	S_{Pt} (μV K^{-1}) at 280 K
Pt 1	134	…	…	…	…	…	−0.6 ± 0.4
Pt 2	134	400	24 ± 2	0.05 ± 0.01	−2.6 ± 0.1	9.2 ± 0.8	−2.3 ± 0.3
Pt 3	197	…	12 ± 1	0.020 ± 0.005	−1.1 ± 0.1	10.9 ± 1.3	−0.7 ± 0.1
Pt 4	197	400	35 ± 2	0.05 ± 0.01	−4.7 ± 0.1	7.4 ± 0.5	−4.7 ± 0.2
Bulk	…	…	47 ± 2	0.09 ± 0.01	−4.8 ± 0.1	9.8 ± 0.5	−4.8 ± 0.1

The Seebeck fit and measurement results are given in Fig. 5(b). The phonon drag peak appears between bath temperatures of 65 K and 75 K. A possible reason for the deviation of the Seebeck fit from the measurement results below 50 K is that the phonon drag part is very sensitive to impurities.[14,28,38] The Seebeck fit provides different parameters, which are given in Table III.

The thermodiffusion part is described by the fit parameter F_{diff}. The platinum films without heat treatment have the smallest thermodiffusion contribution to the absolute Seebeck coefficient, which can be attributed to an increased scattering rate at grain boundaries. The fit parameter of the thermodiffusion part of Pt 2 (134 nm, with heat treatment) is $F_{diff,Pt2} = (-2.6 \pm 0.1)\,\mu V\,K^{-1}$ and of Pt 4 (197 nm, with heat treatment) is $F_{diff,Pt4} = (-4.7 \pm 0.1)\,\mu V\,K^{-1}$. This difference can be explained by increased size effects like surface scattering in Pt 2. The thermodiffusion part of Pt 4 and bulk have nearly the same temperature dependence and magnitude, and it seems that Pt 4 reaches the upper limit of the thermodiffusion part, which is provided by the bulk material.

Compared to the thermodiffusion part, the phonon drag part vanishes at high bath temperatures. F_{ph} estimates the strength of the phonon drag on the absolute Seebeck coefficient. Pt 3 (197 nm, without heat treatment) has the lowest value of the fit parameter $F_{ph,Pt3} = (24 \pm 2)\,\mu V\,K^{-1}$. This value increases with increasing film thickness and with additional heat treatment and reaches its maximum for the bulk material with $F_{ph,bulk} = (47 \pm 2)\,\mu V\,K^{-1}$.

The ratio $|F_{ph}/F_{diff}|$ of bulk and of the thin films is approximately 10, except for Pt 4 (197 nm, with heat treatment), which is slightly lower. This ratio indicates that the thermodiffusion and phonon drag part are reduced by nearly the same factor, when the film thickness is decreasing. To further illustrate that the thermodiffusion and the phonon drag part are related to each other, we introduce F_τ, which gives the ratio of the scattering time of the electron-phonon and phonon-phonon interaction and determines the γ-factor. The γ-factor, see Eq. (14), is a number between 0 and 1, which depends on the interaction between phonons and electrons. For $T \ll \Theta_D$, $\gamma \approx 1$, means that electron-phonon interaction is dominant compared to the phonon-phonon interaction. The phonon-phonon interaction is dominant compared to that of electron-phonon for $\gamma \approx 0$.

The γ-factor as a function of temperature for thin films and bulk is given in Fig. 6. For all temperatures apply $\gamma_{film} > \gamma_{bulk}$. This means that there is an increased amount of the electron-phonon interaction compared to the phonon-phonon interaction in the thin films than that in the bulk. The influence of the phonon drag part on the absolute Seebeck coefficient dominates in thin films compared to the bulk. For example, the thermodiffusion part of Pt 3 is reduced by 77% toward bulk, resulting in a significant effect of the phonon drag part even at room temperature. This difference can be explained by the inner and outer interfaces of the thin films and the resulting grain boundary scattering.

Decreasing temperatures lead to an increase of γ_{film} and γ_{bulk}. This indicates that the electron-phonon interaction is becoming more dominant compared to the phonon-phonon interaction. At temperatures below 50 K, the thermodiffusion part tends to 0, and the γ-factor tends to 1. The reason for this behavior can be attributed to the phonon-phonon interaction, which is negligible compared to the electron-phonon interaction.

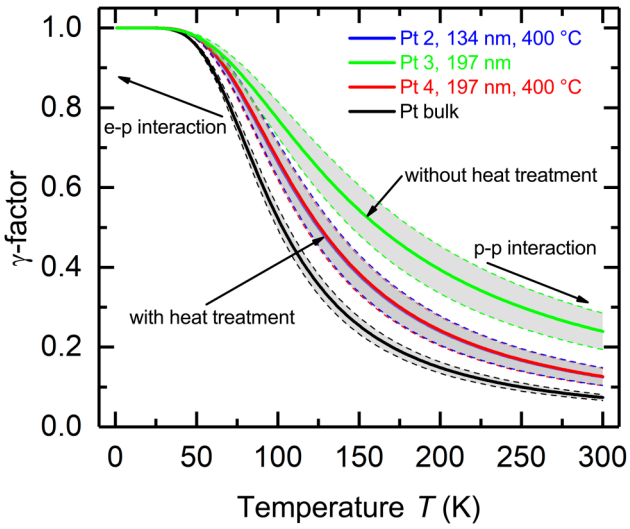

FIG. 6. γ-factor. The panel shows the γ-factor of thin platinum films as sputtered and with heat treatment and bulk material as a function of bath temperature. The γ-factor is determined by the electron-phonon (e-p) and phonon-phonon (p-p) interaction. The gray shaded area around the solid lines marks the uncertainty. $\gamma = 1$ means that the electron-phonon interaction compared to the phonon-phonon interaction is dominant. $\gamma = 0$ means that the phonon-phonon interaction compared to the electron-phonon interaction is dominant. The curves of Pt 2 and Pt 4 have a similar temperature dependence and are lying on top of each other.

Pt 2 (134 nm, with heat treatment) and Pt 4 (197 nm, with heat treatment) have the same γ-factor but different absolute Seebeck coefficients, indicating that the ratio of electron-phonon interaction compared to the phonon-phonon interaction is the same but the absolute amount of electron-phonon and phonon-phonon interaction is larger in thicker platinum films with heat treatment, because the essential limitation is no longer caused by grain boundaries, but by the film thickness.

V. CONCLUSION

In this work, we performed thermoelectric and structural characterizations of thin sputtered platinum films. The influence of heat treatment and film thickness on the electrical conductivity and the absolute Seebeck coefficient were investigated. An additional heat treatment and a larger film thickness increase the crystal quality of sputtered platinum films. The electrical conductivity and the absolute Seebeck coefficient are reduced compared to the bulk due to size effects like surface and boundary scattering. We find that structural properties like grain size and film thickness, which limit the electron mean free path, influence the absolute Seebeck coefficient. For the phonon drag part of the absolute Seebeck coefficient, the electron-phonon interaction compared to the phonon-phonon interaction plays a more dominant role in thin films than in bulk. If the mean free path of thin metallic films is in the order of the film thickness, the absolute Seebeck coefficient of bulk is no more valid. This has to be taken into account, when using thin platinum films as a reference material for the determination of the absolute Seebeck coefficient. Due to the influence of the microstructure, metallic interconnects can be tailored in a way, that the relative Seebeck coefficient can be reduced to zero, which is interesting for low-noise applications.

ACKNOWLEDGMENTS

We acknowledge partial financial support by the German Science Foundation (No. DFG-SPP1386).

REFERENCES

[1]J. Machin, D. Tucker, and J. V. Pearce, "A comprehensive survey of thermoelectric homogeneity of commonly used thermocouple types," Meas. Sci. Technol. **29**, 075418 (2018).
[2]A. M. Burke, D. J. Carrad, J. G. Gluschke, K. Storm, S. Fahlvik Svensson, H. Linke, L. Samuelson, and A. P. Micolich, "InAs nanowire transistors with multiple, independent wrap-gate segments," Nano Lett. **15**, 2836 (2015).
[3]M. S. Dresselhaus, G. Chen, M. Y. Tang, R. Yang, H. Lee, D. Wang, Z. Ren, J.-P. Fleurial, and P. Gogna, "New directions for low-dimensional thermoelectric materials," Adv. Mater. **19**, 1043 (2007).
[4]R. Venkatasubramanian, E. Siivola, T. Colpitts, and B. O'Quinn, "Thin-film thermoelectric devices with high room-temperature figures of merit," Nature **413**, 597 (2001).
[5]M. V. Daniel, M. Lindorf, and M. Albrecht, "Thermoelectric properties of skutterudite $CoSb_3$ thin films," J. Appl. Phys. **120**, 125306 (2016).
[6]A. I. Hochbaum, R. Chen, R. D. Delgado, W. Liang, E. C. Garnaett, M. Najarian, A. Majumdar, and P. Yang, "Enhanced thermoelectric performance of rough silicon nanowires," Nature **451**, 163 (2008).
[7]D. Kojda, R. Mitdank, M. Handwerg, A. Mogilatenko, M. Albrecht, Z. Wang, J. Ruhhammer, M. Kroener, P. Woias, and S. F. Fischer, "Temperature-dependent thermoelectric properties of individual silver nanowires," Phys. Rev. B **91**, 024302 (2015).
[8]J. Kim, G. Kim, J.-H. Bahk, J.-S. Noh, and W. Lee, "Enhanced thermoelectric properties in Bi/Te core/shell heterostructure nanowires through strain and interface engineering," Nano Energy **32**, 520 (2017).
[9]D. Kojda, R. Mitdank, A. Mogilatenko, W. Töllner, Z. Wang, M. Kröner, P. Woias, K. Nielsch, and S. F. Fischer, "The effect of a distinct diameter variation on the thermoelectric properties of individual $Bi_{0.39}Te_{0.61}$ nanowires," Semicond. Sci. Technol. **29**, 124006 (2014).
[10]Z. Wang, S. S. Adhikari, M. Kroener, D. Kojda, R. Mitdank, S. F. Fischer, W. Toellner, K. Nielsch, and P. Woias, "Electrical conductivity and Seebeck coefficient measurements of single nanowires by utilizing a microfabricated thermoelectric nanowire characterization platform," in *IEEE 26th International Conference on Micro Electro Mechanical Systems (MEMS)* (IEEE, Pscataway, NJ, 2013), Vol. 508.
[11]S. H. Moosavi, D. Kojda, M. Kockert, S. F. Fischer, M. Kroener, and P. Woias, "The effect of the MEMS measurement platform design on the Seebeck coefficient measurement of a single nanowire," Nanomaterials **8**, 219 (2018).
[12]V. Linseis, F. Völklein, H. Reith, P. Woias, and K. Nielsch, "Platform for in-plane ZT measurement and Hall coefficient determination of thin films in a temperature range from 120 K up to 450 K," J. Mater. Res. **31**, 3196 (2016).
[13]G. Brändli and J. L. Olsen, "Size effects in electron transport in metals," Mater. Sci. Eng. **4**, 61 (1969).
[14]R. P. Huebener, "Size effect on phonon drag in platinum," Phys. Rev. **140**, 490 (1965).
[15]R. P. Huebener, "Thermoelectric size effect in pure gold," Phys. Rev. **136**, 1740 (1964).
[16]W. F. Leonard and H.-Y. Yu, "Thermoelectric power of thin copper films," J. Appl. Phys. **44**, 5320 (1973).
[17]H.-Y. Yu and W. F. Leonard, "Thermoelectric power of thin silver films," J. Appl. Phys. **44**, 5324 (1973).
[18]V. D. Das and N. Soundararajan, "Size and temperature effects on the Seebeck coefficient of thin bismuth films," Phys. Rev. B **35**, 5990 (1987).
[19]D. K. C. MacDonald, *Thermoelectricity—An Introduction to the Principles* (Dover Publications, Mineola, New York, 2006).
[20]R. P. Huebener, "Phonon scattering by lattice vacancies in platinum," Phys. Rev. **146**, 490 (1966).
[21]R. W. G. Wyckoff, *Crystal Structures* (Interscience Publisher, New York, 1963).
[22]P. Scherrer, "*Bestimmung der Groesse und der inneren Struktur von Kolloidteilchen mittels Röntgenstrahlen* (Nachrichten von der Königlichen Gesellschaft der Wissenschaften zu Göttingen, 1918), Vol. 2, p. 98.
[23]C. Weber, L. Pithan, A. Zykov, S. Bommel, F. Carla, R. Felici, C. Knie, D. Bleger, and S. Kowarik, "Multiple timescales in the photoswitching kinetics of crystalline thin films of azobenzene-trimers," J. Phys. Condens. Matter **29**, 434001 (2017).
[24]N. Stojanovic, D. H. S. Maithripala, J. M. Berg, and M. Holtz, "Thermal conductivity in metallic nanostructures at high temperature: Electrons, phonons, and the Wiedemann-Franz law," Phys. Rev. B **82**, 075418 (2010).
[25]R. B. Belser and W. H. Hicklin, "Temperature coefficients of resistance of metallic films in the temperature range 25° to 600 °C," J. Appl. Phys. **30**, 313 (1959).
[26]W. F. Leonard and R. L. Ramey, "Temperature coefficient of resistance in thin metal films," J. Appl. Phys. **37**, 3634 (1966).
[27]L. L. Kazmerski, D. M. Racine, and M. S. Ayyagari, "Temperature coefficient of resistance in ultrathin metal films," J. Appl. Phys. **46**, 2658 (1975).
[28]R. P. Huebener, "Thermoelectric power of lattice vacancies in gold," Phys. Rev. **135**, A1281 (1964).
[29]M. C. Salvadori, L. L. Melo, A. R. Vaz, R. S. Wiederkehr, F. S. Teixeira, and M. Cattani, "Platinum and gold thin films deposited by filtered vacuum arc: Morphological and crystallographic grain sizes," Surf. Coat. Technol. **200**, 2965 (2006).
[30]L. L. Melo, A. R. Vaz, M. C. Salvadori, and M. Cattani, "Grain sizes and surface roughness in platinum and gold thin films," J. Metastable Nanocryst. Mater. **20–21**, 623 (2004).

[31]J. S. Agustsson, U. B. Arnalds, A. S. Ingason, K. B. Gylfason, K. Johnsen, S. Olafsson, and J. T. Gudmundsson, "Electrical resistivity and morphology of ultra thin Pt films grown by dc magnetron sputtering on SiO_2," J. Phys. Conf. Ser. **100**, 082006 (2008).
[32]M. Krishnan, E. Valderrama, B. Bures, K. Wilson-Elliott, X. Zhao, L. Phillips, A.-M. Valente-Feliciano, J. Spradlin, C. Reece, and K. Seo, "Very high residual resistivity ratios of heteroepitaxial superconducting niobium films on MgO substrates," Supercond. Sci. Technol. **24**, 115002 (2011).
[33]B. D. Hennings, D. G. Naugle, and P. C. Canfield, "Thermal transport of the single-crystal rare-earth nickel borocarbides RNi_2B_2C," Phys. Rev. B **66**, 214512 (2002).
[34]P. K. Das and A. Thamizhavel, "Crystal growth and magnetic properties of equiatomic CeAl," J. Phys. Conf. Ser. **592**, 012009 (2015).
[35]X. Zhang, H. Xie, M. Fujii, H. Ago, K. Takahashi, T. Ikuta, H. Abe, and T. Shimizu, "Thermal and electrical conductivity of a suspended platinum nanofilm," J. Appl. Phys. **86**, 171912 (2005).
[36]M. Cutler and N. F. Mott, "Observation of Anderson localization in an electron gas," Phys. Rev. **181**, 1336 (1969).
[37]C. T. Walker and R. O. Pohl, "Phonon scattering by point defects," Phys. Rev. **131**, 1432 (1963).
[38]M. Bailyn, "Phonon-drag part of the thermoelectric power in metals," Phys. Rev. **157**, 480 (1967).